Graphene Oxide Femto Gel Photodetector

by

Dawood Alsaedi

A thesis
presented to the University of Waterloo
in fulfillment of the
thesis requirement for the degree of
Master of Applied Science
in
Electrical and Computer Engineering (Nanotechnology)

Waterloo, Ontario, Canada, 2016

AUTHOR'S DECLARATION

I hereby declare that I am the sole author of this thesis. This is a true copy of the thesis, including any required final revisions, as accepted by my examiners.

I understand that my thesis may be made electronically available to the public.

Abstract

Due to its unique optical (electrical) properties such as wide-range absorbance of wavelength, and high carrier mobility, graphene becomes a promising candidate for photodetector devices. The ability to tune the band gap, scalability of high-throughput production, and low cost-production methods make graphene derivatives, graphene oxide (GO) and reduced graphene oxide (rGO), attractive for light detection applications from deep ultra-violet to far infrared.

Devices that are used for sensing applications such as photodetectors and gas sensors need to be used in ambient environment. Unfortunately, reliability and stability of graphene derivatives-based devices can be significantly affected by ambient molecule species. Moreover, to maximize the utilization of graphene-derivatives properties in photodetector devices, creating a new active material or engineering the design of device structure is needed.

Therefore, to overcome these three factors, we demonstrated some solutions that are reported for the first time. Firstly, for the aim of creating a new active material that works in ambient environment, we developed a hybrid material that consists of graphene oxide femtogel (GFOG) and polymer (poly(methyl methacrylate) PMMA), and demonstrate the effects on the reliability and operational stability of the photodetector. Secondly, we designed and fabricated a GFOG photodetector that has a combination of large GOFG-metal interface area and GOFG-metal end contact in the device's structure for the first time to enhance the responsivity of the device.

Remarkable reliability, high operation stability, and a significant photoresponsivity have been achieved in GOFG/polymer hybrid photodetector compared to GOFG photodetectors. Moreover, compared to other graphene derivatives photodetectors, a fast response time and a high responsivity have been achieved as high as 3.5s and 0.73 A W^{-1} respectively at low power intensity. The change in the sensing mechanism of a polymer-GOFG hybrid photodetector from bolometric to photovoltaic effect is reported for the first time.

In terms of device structure engineering, this could open a new method in engineering the nanodevice structure of electronic devices based on the aqueous solution form of graphene-

derivatives as putting this type of materials between electrodes in nanoscale is quite a challenge. In terms of material, this study opens a new avenue in the engineering of graphene derivatives-based nanosensor and photodetector active material that have high reliability and responsivity which can be operated in ambient environment. Moreover, the fabrication method and the active material of the device can be used in many nanoapplications such as gas sensing and biosensing applications.

Acknowledgements

First of all thanks is due to Allah whom alone made this project easy and possible. Then, I am grateful to my wife for her support, patience and sacrifice. Also, I would like to thank Prof. Mustafa Yavuz and Prof. Omar Ramahi, for their support and guidance throughout the duration of this project. Finally, Dr Kevin Musselman and Dr. Mehrdad Irannejad are thanked for their assistance, discussions, and suggestions that improved this project.

Dedication

To my parents, my wife and my family

Table of Contents

List of Figures

List of Abbreviations

EBL:	Electron beam lithography
Fs:	Femtosecond
I_d:	Drain current
GO:	Graphene oxide
GOFG:	Graphene oxide femto gel
GPH:	Graphene/polymer hybird
1D:	One dimensional
PMMA:	Polymethyl methacrylate
rGO:	Reduced graphene oxide
SEM:	Scanning electron beam
3D:	Three dimensional
2D:	Tow dimensional
0D:	Zero dimension

Chapter 1
Introduction

1.1 Introduction

Even though the use of semiconductor materials dominate in improving optoelectronics applications technology, some drawbacks are still considered as real challenges against improvement. Due to its indirect band gap, silicon has low efficiency in absorbing and emitting light. Moreover, though silicon has a high mobility and long lifetime of excitons [1], the waveguide's wall scattering has a significant impact in increasing the propagation losses in silicon devices [2]. In addition, conventional photodetectors based on IV and III-V semiconductors have limited bandwidth detection since the photon with energy smaller than the band gap can pass through the material without any carrier excitation [3,4]**.** Therefore, hybrid or new materials that can have the same advantages of photonic semiconductors and can overcome the drawbacks are needed. Due to its unique optical and electrical properties such as wide-range absorbance of wavelength[5], high carrier mobility[6,7], significant absorbance of incident light for single layer[8], graphene has received significant attention as a promising candidate for photodetector devices. The zero band gap of graphene allows detection of photons from the ultraviolet to terahertz range [8,9,10,11].

1.2 Graphene

Since graphene was isolated using scotch tape in 2004 by Novoselov's et al. [12], graphene gained tremendous attention among researchers and scientists over the last several years. Graphene is a two-dimensional single layer that is considered as a single isolated-graphite plane [13] which has an atom thickness that is about 0.345 nm. It has a honeycomb lattice structure which consists of carbon atoms bonded with sp_2 bonds [14]. Monolayer, bilayer, and few-layers (from three to ten layers) are the three categories that graphene can be classified in, where each category exhibits different electrical properties [15]. Using graphene, other important carbon allotropes can be formed such as graphite which is formed from stacked graphene layers known as a three dimensional allotrope of carbon. Also, carbon nanotubes which are one dimensional allotropes of carbon result from rolling up graphene sheets. Moreover, wrapping a graphene sheet creates a zero dimension spherical fullerene as shown in figure 1-1 [16].

Remarkable properties have been observed in graphene such as ballistic carrier mobility and mechanical strength; hence, graphene is considered as a promising candidate for many applications. Therefore, a significant number of studies involve it in a variety of research applications that extend from high sensitive gas sensors and ultra-fast photodetectors to preventing metal corrosion and enhancing solar energy harvesting [17,18,19,20].

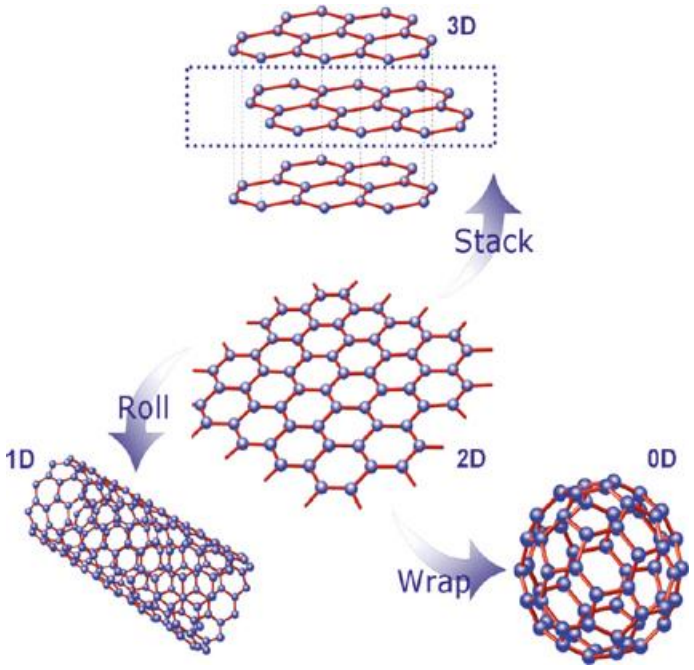

Figure 1-1: Carbon allotropes obtained from 2D graphene. Single layer graphene (center), graphite (top), carbon nanotube (bottom left), and fullerene (bottom right) [16].

1.2.1 Graphene properties

Knowing the chemical structure of graphene is an important factor in determining the reasons behind its outstanding properties. Carbon atoms have four electrons in the last energy state shell and those electrons are what carbon atoms bond to other atoms with. In contrast, graphene has carbon atoms that bond with the adjacent three carbon atoms on single sheet structure via σ bonds. The fourth electron located above or below the sheet in the z-axis connects to another electron forming overlapping bonds called π bonds (fig.1-2) [21]. Due to the stability of the bonds between carbon-carbon atoms, graphene sheet structure has high stability and high mechanical strength that can reach to 1 TPa, which is higher than any other existing material [22].

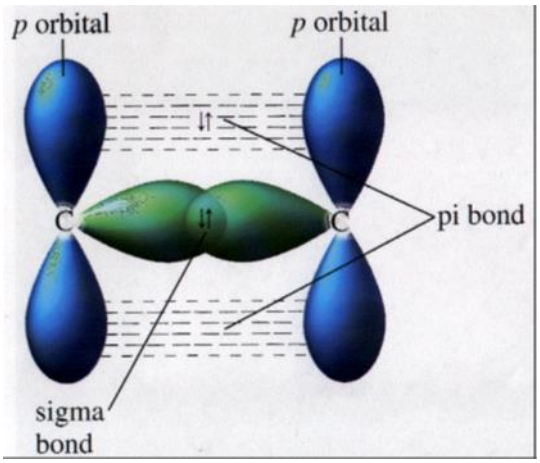

Figure 1-2: Schematic of covalent bonds (sigma) and overlapping bonding (pi) between carbon atoms in graphene. [21]

Near the Dirac point of graphene, the energy-wave factor (E-K) is linear which results in zero effective mass for charge carriers (electrons and holes); hence, a very high carrier mobility (20000 $cm^2/V.s$) can be achieved [6,23]. However, this ballistic mobility could be degraded once graphene is placed on a substrate (SiO_2) due to the scattering of carriers by phonons and charged impurities on the substrate [24,25]. It is worth mentioning that high mobility is the key factor for electronic devices such as photodetectors, gas sensors, and biosensors since it results in a fast response time.

Despite the zero band gap in graphene, it is capable of wide-range absorbance of wavelength [5] which is considered as another important factor in photodetection applications. This mainly can be credited to the intraband and interband optical transitions which will be discussed in detail later. Therefore, graphene is considered as a unique candidate for photodetector applications that can solve the drawback of absorbance range in traditional semiconductor materials [27]. Moreover, graphene exhibits significant absorbance of incident light of approximately 2.3% for single layer which is a remarkably high absorbance for single layer material [8].

1.3 Light detection in graphene

1.3.1 Photon absorbance in graphene

The absorbance of photons in graphene is controlled by two types of transitions. First, intraband optical transition is the transition of charge carriers within the same band (i.e. valence band or conduction band). Intraband transition occurs at incident light with low energy photons such as light that has high wavelength (e.g. terahertz) (fig.1-3 (b)). Second, in contrast, intraband transition is the transition of charge carriers between valence and conduction bands in graphene which happen as a result of absorbing photons with high energy that are produced by low wavelength light such as ultraviolet (UV) (fig.1-3 (c)) [26,27].

When the photon has an energy that is smaller than 2 |Fermi energy (E_F)|, no electron can be excited from valence to conduction band; hence, the photon cannot be absorbed by the graphene sheet (fig.1-3 (a)). However, in this case, electrons can move in the same band range (intraband transition) (fig.1-3 (b)) enhancing the conductivity of graphene and giving a signal of photon absorbance. On the other hand, when a photon has an energy larger than 2 |E_F| electrons can be excited and moved from valence band to conduction band via a process called interband optical transition (fig.1-3 (c)). If the fermi energy is high, no more states are available to allow excited electrons to move from valence to conduction band. [28]

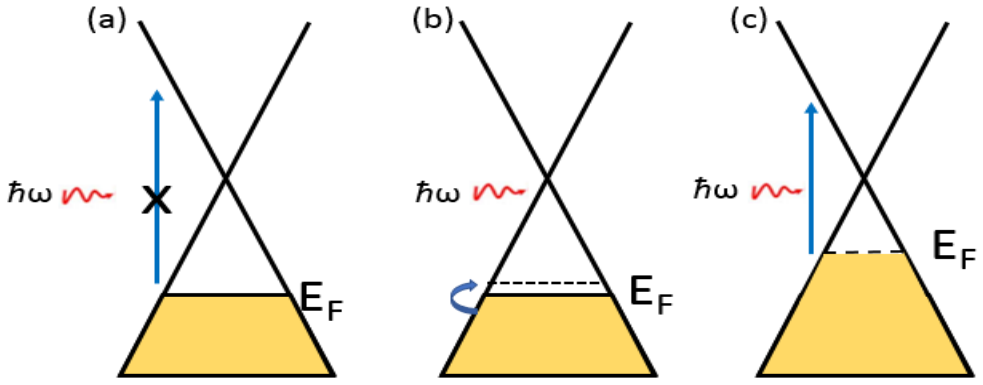

Figure 1-3: Photon absorbance in graphene. $\hbar\omega$ presents the photon's energy. (a) When the photon has a smaller energy than 2 |E_F|, it cannot be absorbed. (b) The intraband transition in valence band. (c) When the photon has a larger energy than 2 |E_F|, it can be absorbed. The blue arrow presents the interband transition.

1.3.2 Sensing mechanism

The sensing mechanism in graphene photodetectors has been investigated intensely to uncover the mechanism behind the remarkable sensitivity in graphene devices. The results of these studies reported three main types of photocurrent sensing mechanisms in graphene devices:

Photovoltaic effect

Under light illumination, photogenerated electron-hole pairs are generated in graphene. These pairs are separated by the internal electric field which only exist at the graphene-electrode interface [5,18,29]. Then the separated carriers are drifted by an external electric field; hence, an increase in charge carriers, resulting in detection action. Figure1-4 (a) shows a sketch of the process of generating and separation of electron-hole pairs in a graphene photodetector.

Photothermoelectric effect

The incident light motivates the difference in temperature in graphene sheets which results in the generation of thermoelectric voltage; hence, photosensitivity can be achieved in graphene photodetectors. Under light irradiation, the photothermoelectric voltage can move through the regions that have different Seebeck coefficients. [27,30,31].

$$V_{PTE} = (S_1 + S_2)\Delta T \qquad (1.1)$$

where V_{TE} is the photothermoelectric voltage, S_1 and S_2 are the Seedbeck coefficients of different regions of graphene with different doping, ΔT is the electron temperature difference between the region under excitation and other areas (fig.1-4 (b))

Bolometric effect

The temperature of graphene can be changed due to light irradiation; hence, the resistance of the active material (graphene) of the photodetector changes. The change in resistance leads to change in conductance of the device which produces a detection signal. Increasing graphene temperature under illumination could be attributed to the weakness of carrier-phonon coupling which leads to fast-carrier heating (fig.1-4 (c)) [32,33].

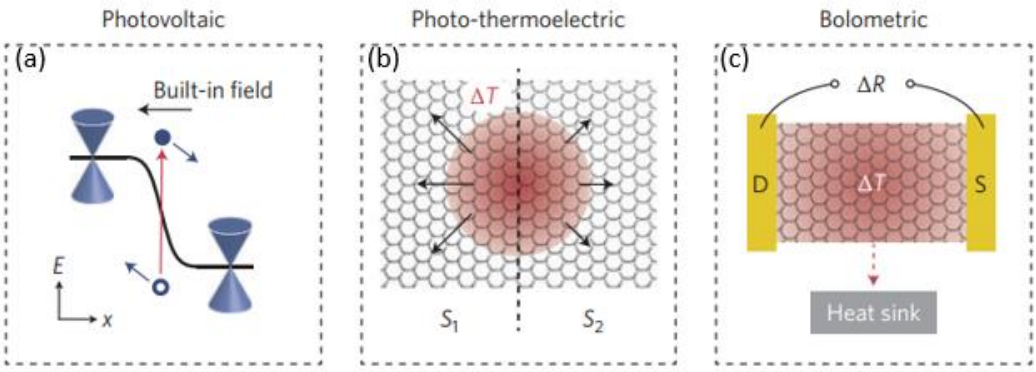

Figure 1-4: Photodetection mechanism in graphene. (a) Photovoltaic effect, (b) photothermoelectric effect, and (c) Bolometric effect. [34]

1.4 Graphene derivatives

1.4.1 Graphene oxide (GO)

Graphene oxide is a graphene sheet functionalized by oxygen which functions such as epoxide and hydroxide at the plane of carbon, and carboxyl groups at the edge of the sheet (fig. 1-5 (a)) [35]. This oxygen functional groups form during the fabrication process of graphene oxide using a variety of techniques. Due to a short fabrication time, easy process, and safe technique, Hummer method becomes the most popular method to produce graphene oxide [36]. In this method, graphite is oxidized using sodium nitrate, sulphuric acid, and potassium permanganate solvents; therefore, the oxygen function bonds to the graphite. Using sonication, graphite oxide layers can be exfoliated to form single and few layers of graphene oxide.

The conductivity of graphene oxide is much less than graphene, which is attributed to the oxygen functional groups that act as scattering sites for charge carriers [37]. However, by controlling the number of oxygen functional groups in the sheet, graphene oxide properties can be changed to achieve the most desirable properties for specific applications.

1.4.2 Reduced Graphene Oxide (rGO)

In the aim of producing graphene from graphene oxide aqueous solution, researchers employ various methods to reduce the number of oxygen functional groups in the graphene oxide sheet. Different techniques have been reported that show that graphene oxide is successfully reduced either by using chemical reactions, thermal reduction, or laser light. The resultant product was graphene with few number of oxygen functional groups (reduced graphene oxide) since these functional groups could not be removed completely from the sheets. Even though reduced graphene oxide has a higher conductivity compared to graphene oxide, its sheets could be affected by the reduction process, hence more defects can present in the sheet's plane. Figure 1-5 (c) shows the difference between reduced graphene oxide and graphene oxide.

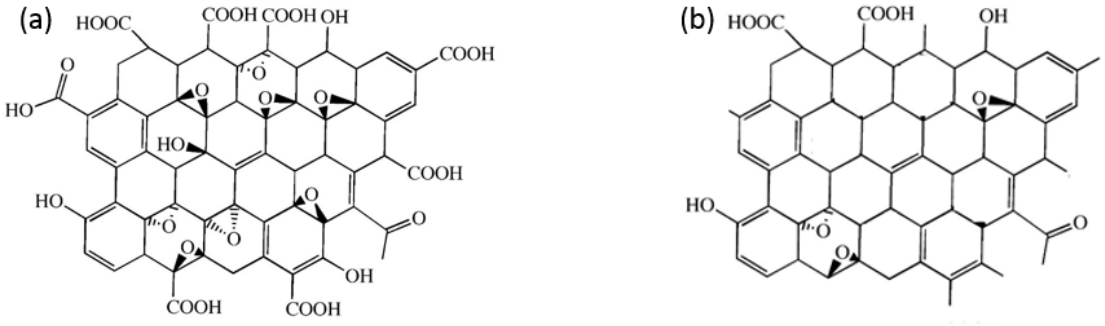

Figure 1-5: Graphene derivative. (a) Graphene oxide and (b) reduced graphene oxide

1.4.3 Using graphene derivatives instead of graphene in photodetection

Despite the drawbacks of graphene derivatives (GO and rGO) electrical properties, compared to intrinsic graphene[L], that results from functionalizing of carbon sheets by oxygen functional

groups, GO and rGO have become more attractive for light detection applications from deep ultra-violet to far infrared [38,39,40,41]. This can be attributed to the advantages presented by graphene derivatives that do not exist in intrinsic graphene. For instance, some studies reported the ability of tuning the band gap of graphene derivatives by optimizing the reduction method [38,39,42,43]. Therefore, the band gab of the active material can be tuned to match the photon energy of the incident light; hence, just the targeted wavelength can be detected. Moreover, scalability of high-throughput production, and low cost-production methods are considered as significant factors since they allow graphene derivatives-based devices to be fabricated in large scale and produced in higher quantity [44,45,46]

Chapter 2
Device fabrication

2.1 Introduction

Using graphene derivatives (graphene oxide (GO) and reduced graphene oxide (rGO)) in the form of gel, solution-process and ink are commonly used in the fabrication of graphene derivatives-based devices. However, to maximize the utilization of graphene-derivatives properties in photodetector devices, creating a new active material or engineering the design of the device's structure is needed. The chemical structure of the graphene-derivatives has been intensively investigated with the aim of improving the responsivity of graphene derivatives-photodetectors. Some studies reported that by controlling the oxygen function defects[1,2] and atomic structure[3], the photocurrent generation was enhanced and a high photoresponse was achieved. Other studies have synthesized graphene derivatives–semiconductor nanoparticles nanocomposite which results in a remarkably fast carrier transport, hence influencing photoresponse[4,5,6]. However, although the active material of graphene derivatives-based photodetectors has been heavily developed, engineering improvements of the device's structure has not received that much interest.

Limited fabrication methods of photodetectors that use GO or rGO as an active material (sensing area) have been reported. Coating the substrate with rGO or GO solution by drop casting method or spin coating to form a thin film, and then patterning the electrodes on the top of this film, is a widely-used method in photodetector fabrication [1-3,7-9]. Sin et al. prepared a vertical junction photodetector that uses GO as the only active material by depositing GO on the top of indium tin oxide and then depositing a gold electrode on top of GO [10]. Moreover, Xiang et al. reported the fabrication method of a photoelectrochemical device fabricated by dropping GO solution on the top of a glass carbon electrode before dipping it into electrolyte solution [11]. However, two important factors that could play a significant role in improving the responsivity and response time of the photodetector were never combined in graphene-derivatives photodetectors: i) increasing the GO-metal interface area since photogenerated (electron-hole pairs) could be separated by an internal electric field created only near the graphene-metal interface [12,13,14] and ii) achieving GO-metal end contact which has been reported to have less contact resistance compared to graphene-metal side contact [12]. Therefore, more investigation in photodetector-structure engineering is needed to improve the device performance and enhance the active material properties.

Here, besides using graphene oxide femto gel for the first time in light detection applications, we report the engineering and fabrication of a graphene oxide femto gel (GOFG) photodetector using GOFG produced using a novel technique as an active material. The device's structure was engineered to contain a large detection area (interdigitated) and GOFG-metal end contact. The GOFG was placed exactly between the interdigitated electrodes without any GOFG above or under the electrodes, which allows us to study the performance of the photodetector that has only an end GOFG-metal interface. It was found that the width of GOFG (channel) can be controlled by adjusting the oxygen plasma etching time. Additionally, the thickness of polymethyl methacrylate (PMMA) and electron beam dose during the lithography process plays a significant role in initializing a window for GOFG etching which will affect the channel's width. This could open up a new method in engineering the structure of electronic devices that are based on aqueous solution forms of graphene-derivatives since putting this type of material between electrodes in nano scale is quite a challenge.

2.2 Experimental methodology

Due to the viscosity of the GOFG, the forming of a thin film has been done by using spin coating technique. The spin coater has a multi speed ability that allows GOFG to spread uniformly on the substrate to form a thin homogeneous film. The lithography of the device's structure was carried out using a scanning electron microscope (SEM), which is known as electron beam lithography (EBL) during the lithography step, to pattern the device's structure in the photoresist (PMMA). After lithography, development of the exposed area of PMMA was removed by Methyl isobutyl ketone (MIBK) which was prepared by mixing 25% of 4-Methyl-2-pentanone with 75% of isopropanol. Due to its capability in depositing metal in nano thicknesses and ability to deposit more than one type of metal under the same vacuum, an electron beam evaporator was used to deposit the interdigitated electrodes of the device.

2.3 Graphene oxide femtogel (GOFG)

2.3.1 Fabrication of GOFG

It is worth mentioning that Graphene oxide femtogel (GOFG) was fabricated and characterized by group colleague, Khaled Ibrahim [15]. Due to the importance of giving a complete picture about the motivation and fabrication of the GOFG photodetector, it is necessary to report the significant points in fabrication and characterization that relate to this project.

A novel fabrication technique has been used to produce GOFG using femto second (fs) laser shined to a high concentration graphene oxide aqueous solution. The solution was exposed to the laser for 7 hours with laser wavelength of about 800 nm, the laser pulse energy irradiating the solution was set at 2mJ, also noting that the pulse duration was 100 fs and the repetition rate was 1 kHz. The laser is directed on untreated graphene oxide solution of ultra-high concentration standing at 6.2 mg/mL. [15].

2.3.2 Characterization of GOFG

As a consequence of the fs laser ablation, the OH absorbance feature entirely disappeared as shown in figure 2-1. That can be attributed to the removal of OH bonds from GOFG in the form of vapor as a result of a long exposure time. Compared to unexposed GO solution, the intensity of the sp^2 bonded C=O bonds were reduced in GOFG. In addition, the absorbance intensity of the C-OH bond was completely reduced in GOFG by increasing the exposure time. The bending C-H bond completely removed from GOFG after 7 hours of exposure. This can be attributed to the dismantling of the weak bonds between C-H and then reactions between OH- ions and the hydrogen ions which forms water vapor.

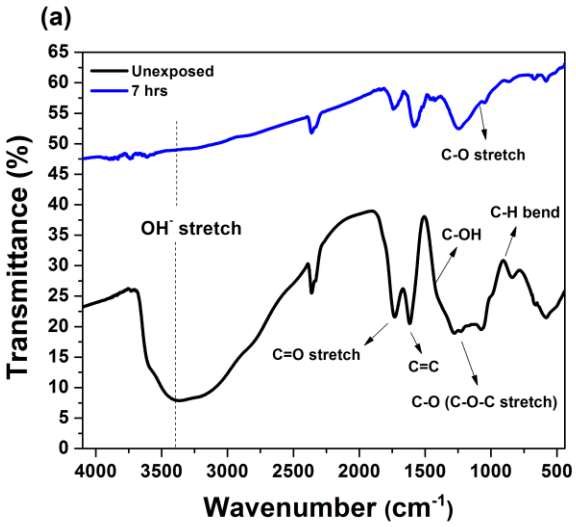

Figure 2-1: The FTIR spectrum of unexposed GO thin film and GOFG film after 7 hours of laser ablation. [15]

In the aim of investigating the chemical structure of both carbon and oxygen atoms in unexposed GO and GOFG, X-ray photoluminescence spectroscopy (XPS) analysis was carried out. Figure 2-2 (b) shows the disappearance of COOH from GOFG after 7 hours of laser exposure which was attributed to the evaporation caused by laser ablation, hence the components of COOH reduced strongly. In unexposed GO, the two main peaks C-C and C-O are not interrelated since graphene oxide sheets are not bonded together (fig.2-2 (a)). In contrast, in GOFG, after 7 hours, the two main peaks are closely interrelated due to the bending

and aggregation of the G sheets. Two main peaks are closely interrelated due to the bending and aggregation of the G sheets. Moreover, compared to unexposed GO, an increase occur in C=C peak and C-O peak which credit to generated of more sp3 hybridization as result of dismantling of the sp2 bonds (figs. 2-2 (a) and (b)).

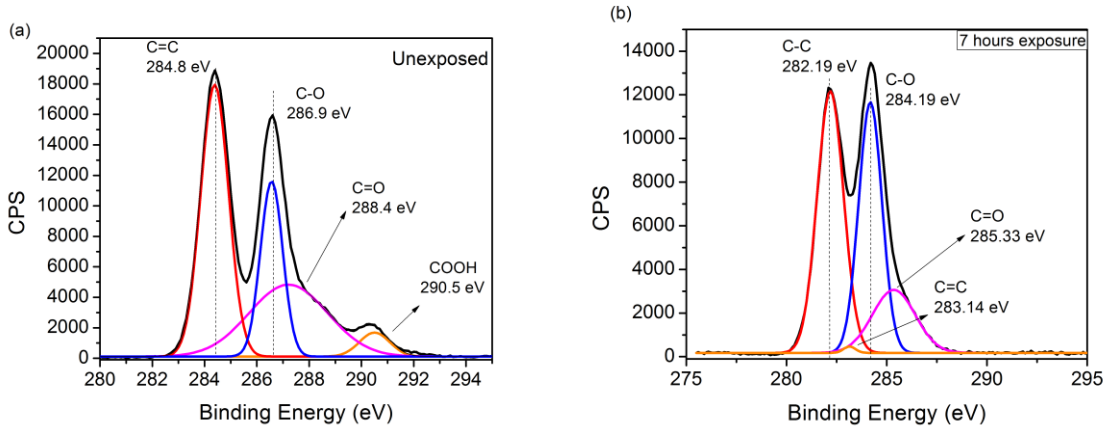

Figure 2-2: The XPS spectrum of GOFG. (a) unexposed GO film (b) GOFG film exposed for 7 hours. [15]

2.4 Device fabrication

2.4.1 Fabrication process

In this device, a graphene oxide sol-gel (GOFG) produced by shining a laser on untreated graphene oxide solution of ultra-high concentration standing at 6.2 mg/mL was used as an active material of an interdigitated photodetector. The solution was exposed to the laser for 7 hours with a pulse energy of 2mJ, pulse duration of 100 fs, repetition rate of 1 kHz, and wavelength of 800 nm. Due to the high viscosity of this gel, it was spin coated on 300nm Si/SiO_2 substrate using gradual-rotation speed. 1000, 2000, 4000, and 6000 rpm were employed respectively for 10s duration for each speed which results in a uniform thin film with a 24nm thickness. Spinning of multi layers of a positive photoresist PMMA to obtain a thick photoresist layer on the GOFG film was followed by baking in a hotplate at 160°C for 10 min to evaporate the solvent. Electron beam lithography was used to shape an interdigitated device

with 25 fingers in each electrode with 1µm distance between each two fingers. Oxygen plasma etching was carried out to remove the entire GOFG film from the exposed and developed PMMA area to ensure GOFG is placed only between the patterned interdigitats. The time of plasma etching could be increased when the distance of channel between fingers was controlled. In this study, 2 mins for 5 times of oxygen plasma etching was performed, resulting in 1µm channel width between adjacent fingers and 1µm finger width. The electrodes (source's and drain's pad and fingers) consist of 0.3 nm Ti and 60 nm Au deposited between the patterned GOFG by electron beam evaporator. To shape the channel and remove unnecessary GOFG that surround the device, a second step of electron beam lithography and oxygen plasma etching were applied as the last step of the fabrication process. Coating the photodetector via PMMA is one more step applied to the device after the first set of characterisations (fig 2-3).

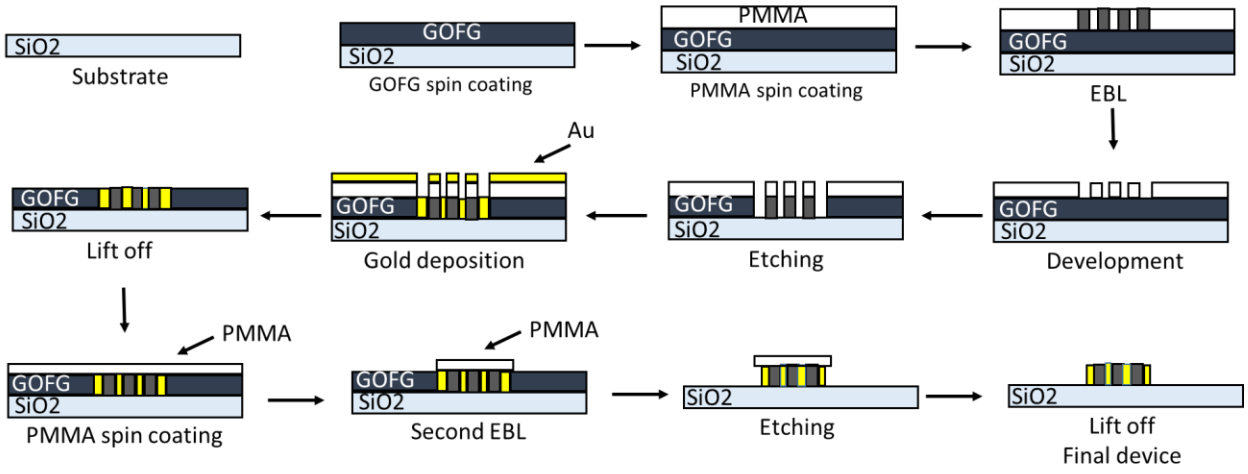

Figure 2-3: The fabrication process of a GOFG photodetector.

2.4.2 Evaluating the vertical etching of GOFG

Since its effectiveness has been reported in etching graphene either vertically [16,17,18] or horizontally [19,20], plasma etching was used to etch GOFG in this photodetector. GOFG needed to be entirely etched vertically in the area between electrodigitates to achieve GOFG-metal end contact. Therefore, to ensure a complete-vertical etching, AFM, an optical

microscope and a Raman spectroscope were employed after different etching times since they are considered to be more effective when combined together to check the availability of GOFG [17]. Figures 2-4 (a), (b), and (c) show optical microscopy images of GOFG after 4, 6, and 8 mins of oxygen plasma etching respectively. As can be seen, 4 and 6 mins were not enough to remove the entire GOFG since some flakes layers were still remaining. However, after 8 mins of etching, GOFG seems to be removed completely (Fig. 2-4 (c)). Atomic-force microscopy (AFM) images exhibit compatible results with optical microscopy images where an 8 min period is considered as a proper etching time for vertical etching (Figs. 2-4 (d), (e) and (f)).

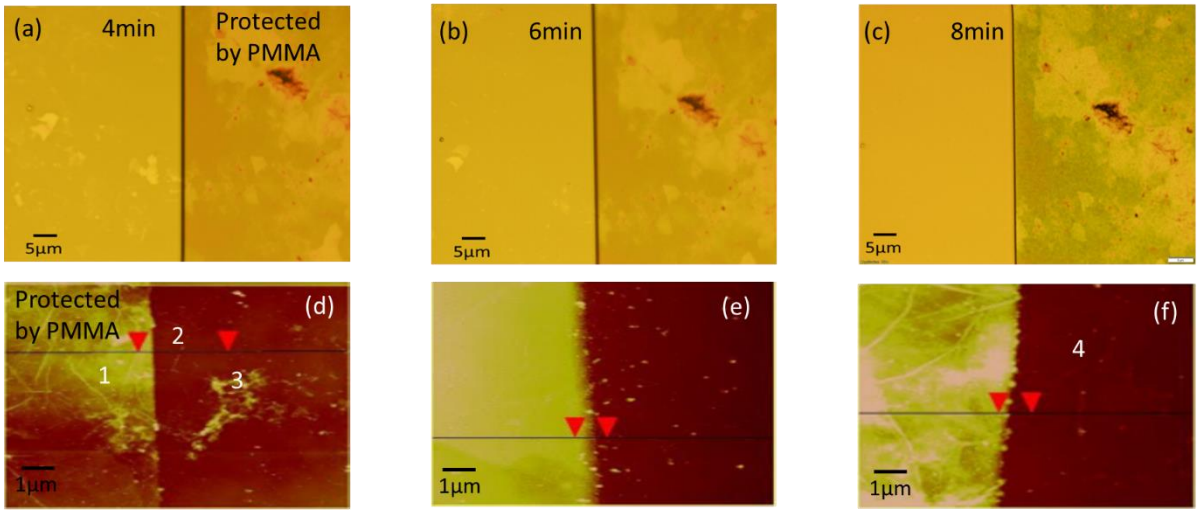

Figure 2-4: Vertical etching of GOFG thin film: (a), (b), and (c) show the optical microscope images of GOFG vertical etching after 4, 6, and 8 minutes respectively. (e), (f), and (g) represent the AFM images after 4, 6, and 8 minutes of GOFG vertical etching respectively.

In further investigation, Raman spectroscopy was employed after every etching time to evaluate the GOFG etching. The Raman spectrum of GOFG film shows G, D peaks which are the two main typical peaks of graphene oxide as shown in figure 2-5 (a) [21,22]. After 4 mins, the spectrum proves the availability of GOFG flakes with lower thickness compared to the GOFG film as a result of partial vertical etching. However, G and D bands totally disappeared after 8 mins which is attributed to the entire etching of GOFG and support the results obtained from the optical microscope and AFM. The thickness of the GOFG film was measured after the completion of the vertical etching and found to be about 24 nm (fig. 2-5 (b)).

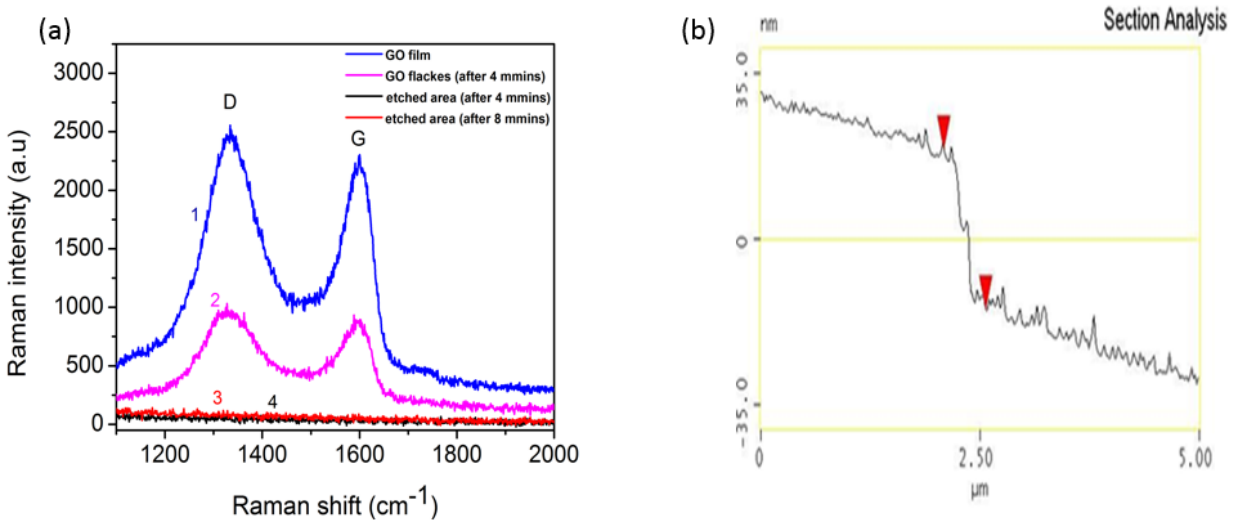

Figure 2-5: Raman spectrum and the thickness of GOFG film. (a) The recorded Raman spectrum of the points that numbered in fig. 2-4 (d) and (f): (1) GOFG film before etching, (2) the remain flakes after 4 mins, (3) the etched area after 4 mins, and (4) after 8 mins. (b) The thickness of GOOFG film after completed etching (about 24 nm).

The final device can be seen in figure 2-6 (a) and the active material that replaces material between the electrodes fingers are shown as a contrast in colour in the enlarged image (fig. 2-6(b)) near the heads of the red arrows.

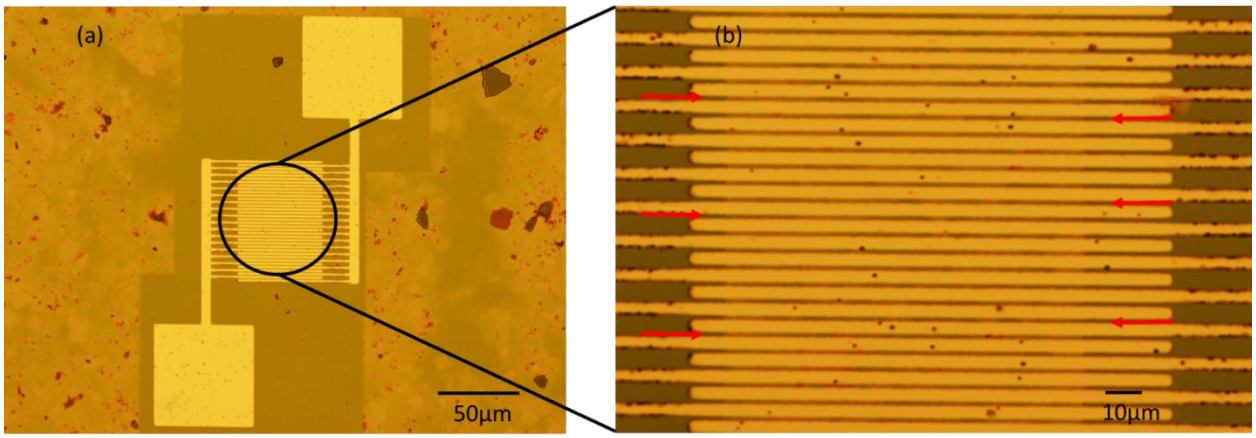

Figure 2-6: The final device. (a) An optical microscope image of the final device. (b) An enlarged image of the interdigitated structure that shows the GOFG placed between electrode fingers as a contrast in colour near the heads of the red arrows.

2.4.3 Controlling the width of GOFG (channel)

During vertical etching, the edges of GOFG were also affected since plasma etching is unidirectional etching. Therefore, the width of GOFH (channel) patterned between the interdigitated electrodes can be controlled once finishing the vertical etching. Figure 2-7 (a) shows the GOFG width as a function of etching time where the relation seems to be almost linear. While the top of GOFG is protected by PMMA, increasing the etching time yields more side etching of GOFG which leads to a decrease in the channel width between two adjacent electrode fingers. Thus, the distance that carriers travel through to reach the electrodes could be reduced, hence that influences the response time of the device[12]. In addition, the thickness of PMMA protecting layers above some areas of GOFG, should be considered to insure the etching effect does not reach the GOFG as we want to keep it as is. Figure 2-7 (a) inset shows the linear relationship between PMMA thicknesses and etching time; consequently, the suitable PMMA thickness could be specified.

It is noted that more factors could affect controlling the width of GOFG. During the fabrication process, PMMA thickness and electron beam dose of electron beam lithography play a significant role in opening an initial-etching window in PMMA layers. The width of that window specifies the stating etching width that applies to GOFG. According to the curves shown in figure 2-7 (b), the increase in PMMA thickness results in wider exposed area of PMMA due to an increase in the forward scattering of electrons, hence a wider window could be opened in PMMA layers. Moreover, for the fixed PMMA thickness, the electron beam dose exposed more area of PMMA once the dose increased, resulting in enlargement of the initialized etching window.

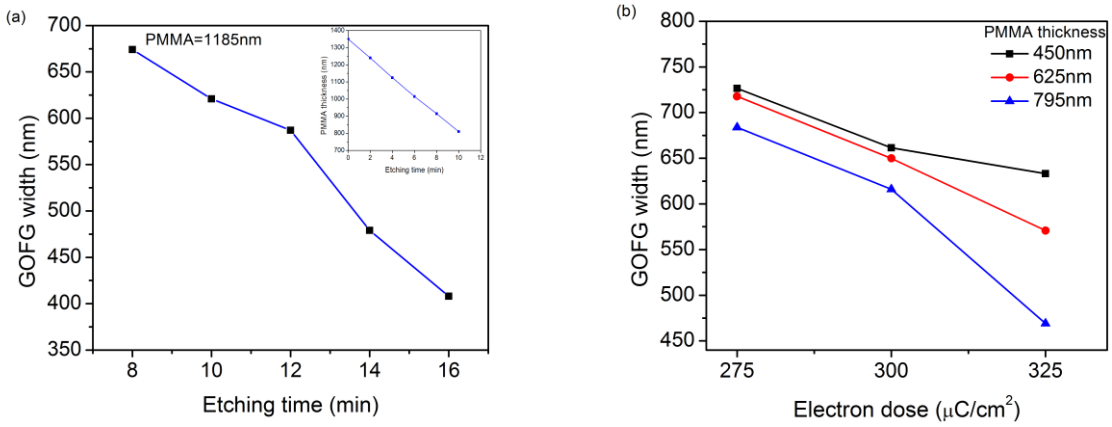

Figure 2-7: Side etching of GOFG film. (a) The side etching of GOFG thin film as a function of oxygen plasma etching time. Inset: PMMA protection layer etching rate as a function of oxygen plasma etching time. (b) The side etching of GOFG thin film as a function of electron dose for different PMMA thicknesses.

2.5 Conclusion

The fabrication of a photodetector with an active material produced by a novel technique was presented for the first time. Toward the utilization of GOFG properties, the device's structure was engineered to achieve a large detection area by increasing the GOFG-metal interface, and minimizing the contact resistance by fabricating the GOFG-metal end contact. During fabrication, the major factors that dominate the controlling of the GOFG channel width (oxygen plasma etching time, PMMA thickness and electron dose) and their effects were investigated in detail. In terms of device structure engineering, this could open a new method in engineering nanodevice structures of electronic devices based on the aqueous solution form of graphene-derivatives since putting this type of material between electrodes in nanoscale is quite a challenge. Moreover, In terms of material, this study opens a new avenue in engineering the graphene derivatives-based nanosensors and photodetectors active material that have high reliability and responsivity which can be operated in ambient environment. Also, the fabrication method and the active material of the device can be used in many nanoapplications, such as, gas sensing and biosensing applications.

Chapter 3
Enhancing Of Photosensitivity and Operation Stability of GOFG Photodetector Utilizing Polymeric-Coating Layer

3.1 Introduction

Devices used for sensing applications such as, photodetectors and gas sensors need to be used in ambient environment; unfortunately, operation stability of graphene-base devices can be significantly affected by ambient molecule species. During fabrication, the sheet of carbon can miss some atoms which causes defects to occur in its body. These defects play a significant role in interaction between the sheet and ambient environment since more sites become available for bonding with other molecule species in the surrounding environment [1,2]. Consequently, water vapour molecules are absorbed, which are considered as a dipolar molecules, in the device's sensing area; therefore, a remarkable change can affect the electrical properties of the devices resulting in unstable sensing operation [1,3,4,5].

To address this problem, coating the sensing area (graphene or graphene derivatives) to prevent any interaction with ambient during operation can be an acceptable solution. However, two important requirements should be considered in the coating layer before applying this step: first, the medium to be measured should not be retarded by the coating layer. Second, ensuring no affect for the electrical properties such as mobility which can deteriorate due to coating-layer doping. Stable operation of a graphene inverter has been reported by Yun et al. under

ambient environment by coating an inverter-graphene channel with a polymeric layer [6]. Moreover, it has been reported that putting a thin polymer layer between the channel and the dielectric or between the channel and the substrate enhances the mobility of the graphene transistor [7,8]. This stability with polymeric covering compared to exposed devices is attributed to two main factors: i) ability of polymer to decrease the hystrisise [1,3], caused by absorbance of water molecules from the air [2,3,4], hence preventing the deterioration of electrical properties and ii) charge impurities and surface phonons that are mainly responsible for carrier scattering can be screened by polymer which increases the mobility [7,8,9] and prevents balanced electron and hole scattering [6]. These two factors result from the polymeric shield that prevents ambient molecules from reaching the sensing area and significant bonds created between polymer coating layer and sensing area in graphene-based devices and substrates [3,6]. Although the consequences of encapsulated graphene-based devices with polymer have been reported for some devices, such as transistors, inverters, and thermal detectors, although its effects in photodetector stability, sensitivity and sensing mechanism have not yet been reported [3,6,7,8].

3.2 Experimental methodology

In order to evaluate the value of change in GOFG photodetector properties before and after adding the polymeric layer to the sensing area, electrical and photocurrent measurements were carried out for the same device with and without the polymeric layer. Due to the unavailability of photomeasurement equipment on campus, a special setup was arranged to characterize the devices. A probe station with very small probe tips was used to connect probes to the photodetector's electrodes. The supply for these probes and the measurements were provided by a parameter analyser (Keithley 2400 SCS). Two types of illumination sources were used as incident-testing light: white light and visible light. The white light was defined as the light that has all wavelengths, while visible light has a specific wavelength. The white light of the microscope was the available choice, and three visible light sources with different wavelengths (blue 465 nm, green 525nm and red 625 nm) were purchased from Super Bright LEDs. The

LEDs could be operated at different voltages, required to measure the photocurrent under different light intensities. The light sources were powered using a source measure unit (Keithley 2400 SourceMeter). Since different light intensities were used during the experiments, the intensity of light was measured using a photometer to connect the data to what was obtained from the parameter analyser.

3.3 The effects of polymeric-coating layer

3.3.1 Enhancing the photosensitivity

Using a low power light source adds more ability of PMMA in improving the sensitivity of GOFG photodetectors. Due to the relatively low power of the light, interaction with ambient molecules, and trapping of carriers by oxygen functional groups [10,11], it is difficult for the uncoated photodetector (GOFG photodetector) to detect the light; hence, no change in conductivity could be noticed. However, a remarkable improvement in light sensitivity occurs by covering the photodetector with PMMA (GOFG/polymer hybrid photodetector(GPH)) for the same light power as in figure 3-1.

The significant interaction between PMMA and GOFG can be attributed to the hydrogen bonds created between hydroxyl groups of GOFG and the carbonyl group of PMMA and electrostatic interaction between negatively charged oxygen functional groups of GOFG and positively charged amine groups on the head of the PMMA chain [12]. In addition, more hydrogen bonds can be formed between the ester group of PMMA and silanol groups on SiO2 [3]. Taking into account the hydrophobicity of the PMMA can avoid the reaching of the ambient species to the sensing area on GOFG photodetector, and evaporation of water from GOFG during baking of PMMA [3], all the above contribute to suppression of hysteresis [1,3] and screening of carrier-scattering causes [3,7,8]. Consequently, an improvement in stability of the device operation and photosensitivity for the incident light detection in GOFG photodetector can be achieved.

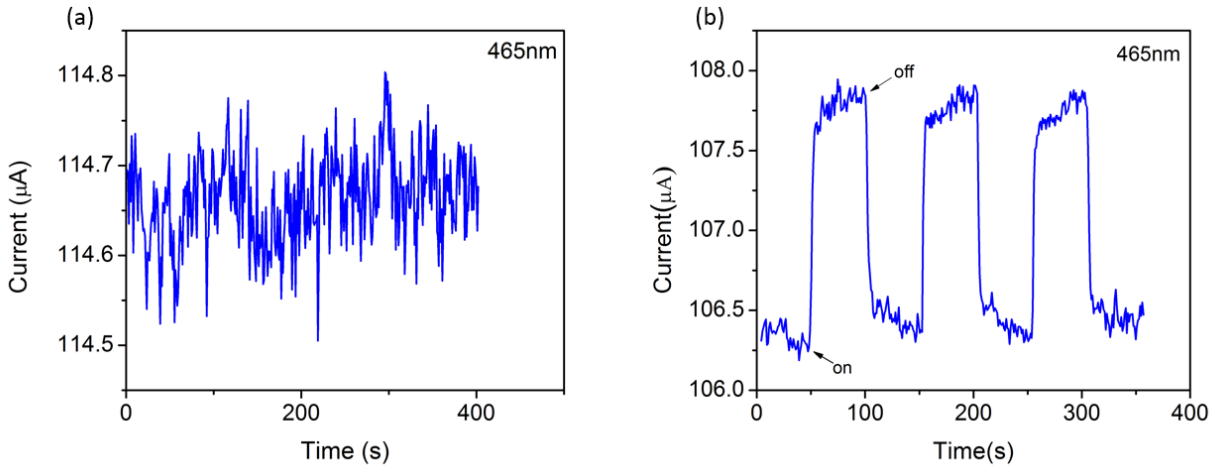

Figure 3-1**:** Temporal photoresponse under visible light (blue 465nm) for (a) GOFG photodetector and (b) GPH photodetector. (V_{ds} =100 mV).

3.3.2 Operation stability

3.3.2.1 Operation stability with sweeping voltage

In order to examine the stability of the device under ambient conditions, we first measured the drain current (Id) of the device as a function of a sweep-bias voltage. As shown in figure 3-2 (a) the Id value of the GOFG photodetector that has an ambient-exposed sensing area tends to increase slightly after every measurement. Increasing by 0.03mA and 0.02mA after 5 and 10 minutes respectively at the beginning and the ending of the curve (fig. 3-2 (b)), is attributed to evaporation of the water molecules that were absorbed by bonding sites at carbon sheet's defects [1,2], from GOFG due to current annealing. In contrast, the GPH photodetector shows more stable Id current with about 93% less change in value compared to an uncovered device (fig. 3-2 (c) and (d)). Instead of increasing, the Id current has a very minor decreasing in Id current with repeating operation which proves that the role of PMMA is preventing penetration of the ambient species from reaching to the photodetector's sensing area [3]. In addition, the decreasing of Id in GPH photodetector could be attributed to the heating caused by passing-though current resulting in an increase of the resistance. It is worth mentioning that the coating the device by PMMA has been done under ambient conditions at room temperature without

any vacuum or annealing which keeps the absorbed water species in the GOFG after coating. However, baking the device after coating at 160°C for 10 minutes can evaporate most of water molecules from the sensing area [3].

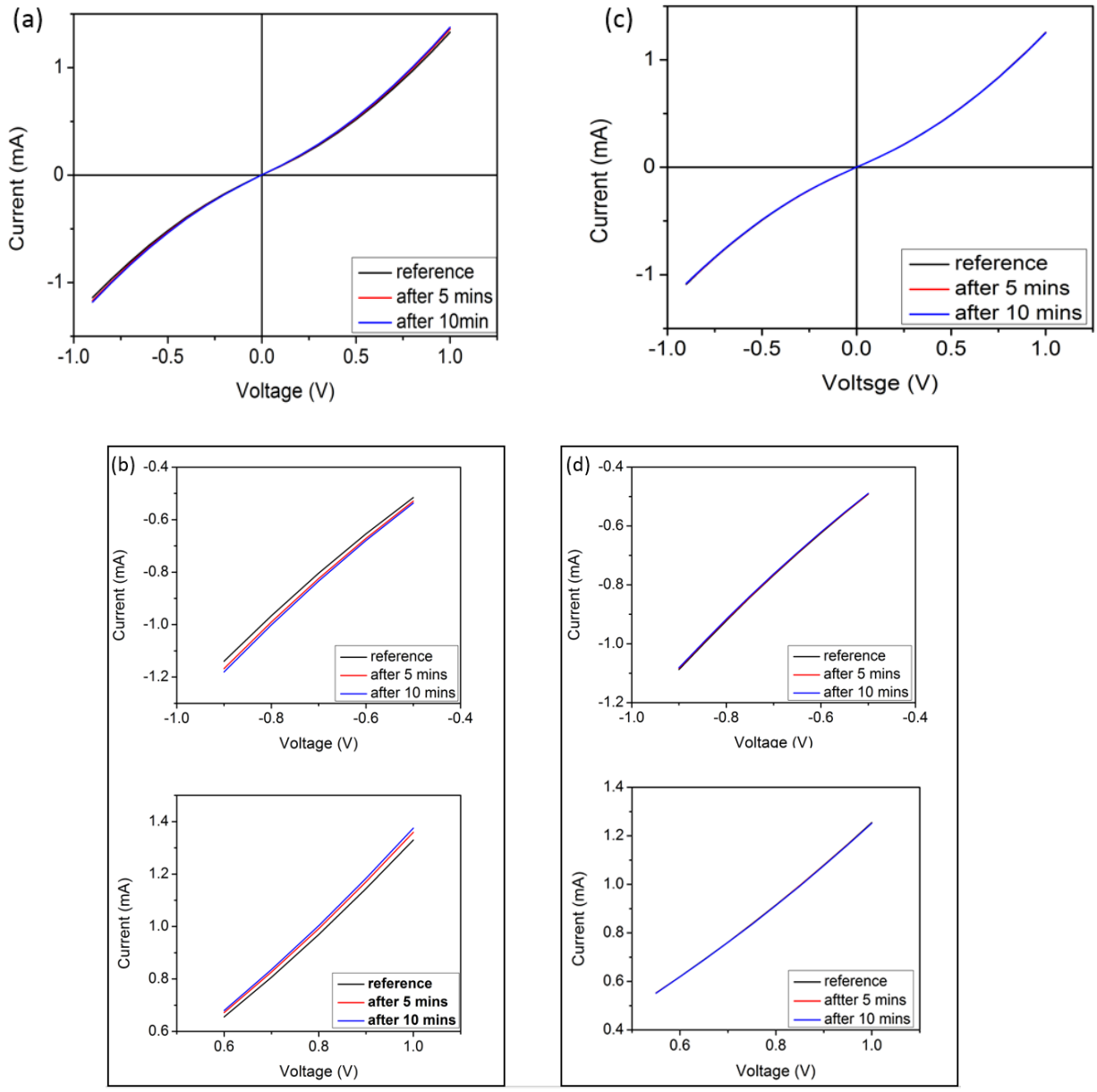

Figure 3-2**:** I_{ds}-V_{ds} curves under dark. (a) GOFG photodetector I_{ds}-V_{ds} curve (full curve). (b) Enlarged pictures of the beginning (up) and the ending (down) of the curve at (a). (c) GPH photodetector I_{ds}-V_{ds} curve (full curve). (d) Enlarged pictures of the beginning (up) and the ending (down) of the curve at (c). at V_g= 0 V

3.3.2.2 Operation stability with fixed voltage

Toward further investigation of the device's operational stability, investigation of the current stability of the device versus fixed bias voltage is necessary since photosensing testing is mostly performed at a fixed bias voltage to measure the photocurrent [10-17]. As shown in figure 3-3 (a), at 200mV, GOFG photodetector shows a noisy unstable current that varies from 164.3µA to 165.57µA over 400s. That probably is caused by two main reasons: i) absorbed water molecules in GOFG which act as charge carrier traps [1,2,3] and ii) interaction between the active area in the device with ambient environment species which may increase the number of oxygen atoms that bond to the carbon sheet, resulting in more carrier trapping [1,10,11]. Even though repeating the operation of the device several times improves the stability of Id, it still increases over time as shown in figure 3-3 (a) as a consequence of evaporation of water molecules as mentioned above. Although unlikely, the GPH photodetector shows a remarkable stability either from the first operation or after many testing operations, showing the effect of coating the polymeric layer in device operation stability as plotted in figure 3-3 (b).

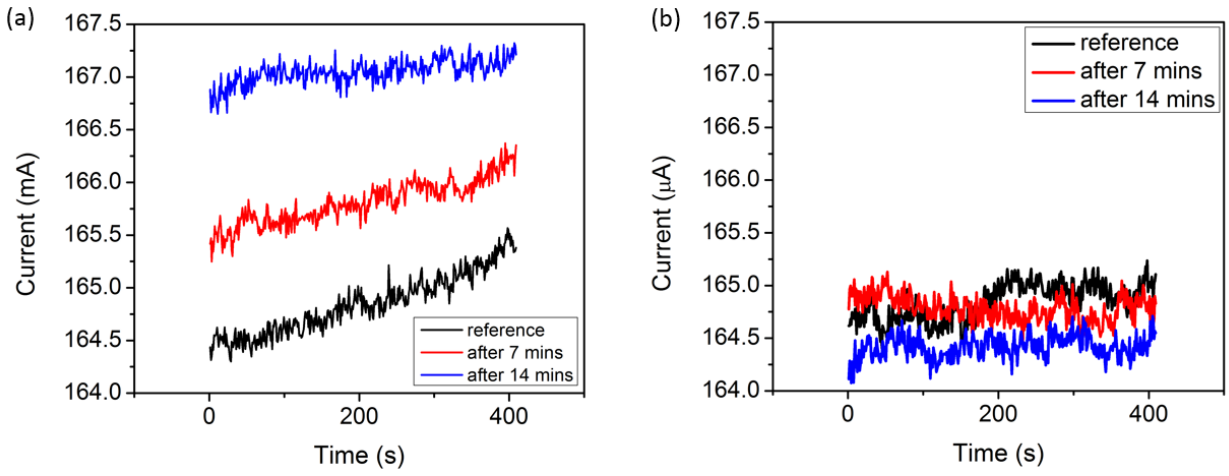

Figure 3-3**:** I_{ds} as a function of fixed V_{ds} (V_{ds} =200 mV) for GOFG device (a) and GPH device (b) showing the operation stability over repeating operations of the device before and after PMMA coating.

3.3.3 Change in sensing mechanism

The sensing mechanism of both devices has been demonstrated for the aim of further investigation into the effect of PMMA coating layers in photodetector sensing. Two different sensing mechanisms were observed in GOFG and GPH devices. In GOFG photodetector, once the illumination source was turned on, the value of current decreases until the light was turned off. After turning off, if the test is done during unstable current stage that is shown in figure 3-3 (a) (reference curve), the current tends to return to its original value before incident of light figure 3-4 (a), while the current remains at the same value reached (fig.3-4 (b)) if the illumination test was done when the device has a more stable Id as in figure 3-3 (a) (after 14 mins curve). However, in both cases, the sensing mechanism shows bolometric behaviour as reported in some graphene photodetectors [18,19]. It is noteworthy that there is a very short increase in Id at the moment of switching the light on. However, in GPH photodetector, Id increases immediately when the light is turned on and returns to its original value when the light is switched off, showing photovoltaic effect mechanism as shown in figure 3-5. This changing in mechanism behaviour can be explained by the fact that the fabrication method of GOFG using laser ablation leads to a high number of defects in the GO sheet. Therefore, under light radiation, although generating electron-hole (e-h) pairs at GOFG-matel interface [20-23], carbon lattice heating occurs due to the presence of defects, which scatter the charge carriers, causing an increase in lattice temperature [16]. Each case has the opposite effect in terms of electrical transport. While photogenerated increase in the conductivity of the sensing area occurs under the effect of applied bias, lattice heating increases the local temperature leading to resistance increase which affects the conductivity negatively. Therefore, two different sensing mechanisms appear: photovoltaic effect and bolometric effect [16,24] and once one of them overcomes the other, it dominates the sensing mechanism. That explains the short term improvement in Id (conductance) at the moment of switching on the light in the uncoated device as a result of separation of photogenerated (e-h pairs) by an external electric field followed by a quick increase in the resistance due to lattice heating that ends with degradation of the Id value; therefore, the bolometric effect is observed in GOFG photodetector. In contrast,

as a consequence of the PMMA's capability in screening the causes of carrier scattering [7,8,9] including defects, sensing mechanism of GPH device shows dominance in photovoltaic effect.

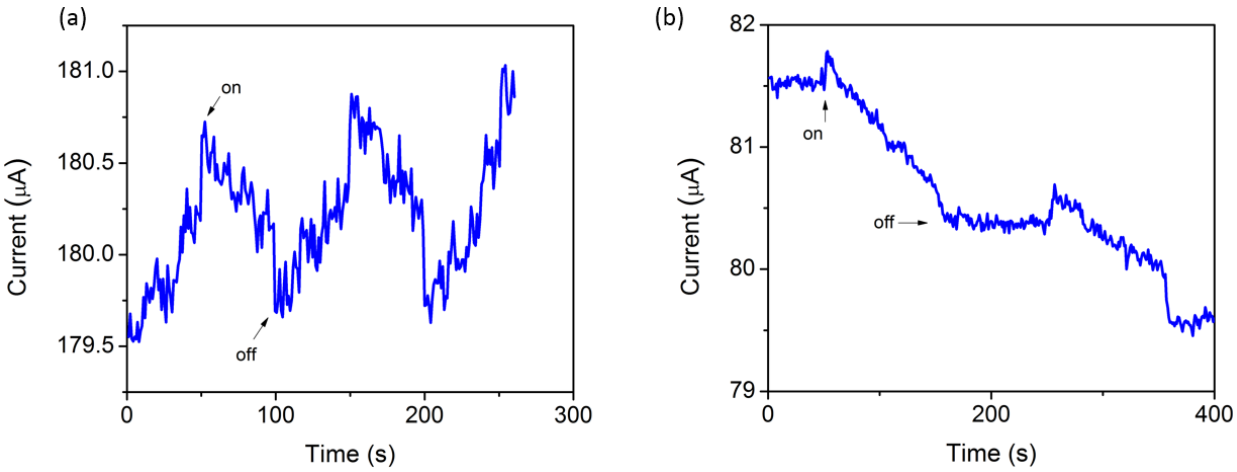

Figure 3-4**:** Photocurrents as a function of time of uncoated GOFG photodetector under white light. (a) before current becomes more stable (like the reference in fig. 3-3 (a)) (V_{ds} =200 mV). (b)After current gets more stability (like "after 20 mins" in fig. 3-3 (a)). (V_{ds} =100 mV)

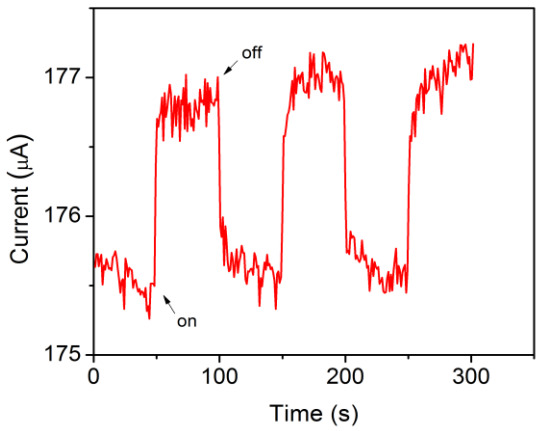

Figure 3-5**:** Temporal photoresponse of GPH photodetector under white light.

(V_{ds} =200 mV)

3.4 Conclusion

It was demonstrated that a thin layer of PMMA can significantly enhance the operational stability, photosensitivity, and sensing mechanism in a photodetector that uses GOFG as an active material. Through the repeating of characterization, a noticeable current stability can be achieved in the GPH device either with sweep or fixed voltage compared to GOFG device. Moreover, the sensing mechanism of the photodetector shows a remarkable change with and without a PMMA-covering layer. While it tends to be a bolometric effect in GOFG device, it shows photovoltaic effect in GPH photodetector. Also, even though there was no sensing, the detection of low power light was achieved after employing a thin layer of PMMA on the sensing area. This study could open a new window in the study of the stability and sensing mechanism of graphene-based devices operating in ambient environment.

Chapter 4
The performance of the GOFG/polymer hybrid photodetector

4.1 Introduction

Electrical and photocurrent measurement are important in showing the performance and the capability of the photodetector. Also, the limitation, the responsivity, the speed, and the application of the device can be determined through these measurements. Therefore, illumination sources with different wavelengths (blue 465 nm, green 525nm and red 625 nm) were used to provide more characterization aspects. In the visible range, a remarkable light detection and fast behaviour was observed for all different visible light wavelengths; hence, a high responsivity was achieved as high as 0.73 A W^{-1} at low power intensity 80 mW/cm^2 which is considered as high responsivity for a graphene oxide photodetector compared to other graphene derivative-based photodetectors. Moreover, the GOFG/polymer hybrid photodetector exhibits an excellent reproducibility under continuous cycling of switching the light source on and off. The device has a high selectivity since it shows a different photocurrent magnitude for different incident light intensity. In addition, a fast time response for both growth and decay time was recorded which put the device among the fastest graphene derivative-based photodetectors.

4.2 Characterization of Photodetector Performance

4.2.1 Photoresponse

The performance of the photodetector in detection of light was investigated in the visible light wavelength range (blue 465nm, green 525nm, red 625nm). Typical I-V characterization of

GOFG/polymer hybrid photodetector in dark (black) and under visible light irradiation (red) at 465 nm with 84mW/cm^2 is plotted in figure 4-1 (a). By sweeping the bias voltage from -1V to 1V, a nonlinear I-V curve resulted, which indicates creating of a Schottky-like barrier in metal-GOFG-metal contact[12] (figure 4-1 (a) inset). The GOFG photodetector shows a remarkable photoresponse on all different visible light wavelengths: blue, green, and red as plotted in figure 4-1 (b), (c), and (d) respectively. The photocurrent increases immediately after turning the light on, and falls quickly to its original value (dark current) once the light was turned off. The increasing in the conductance of the device under incident light is mainly credited to photogenerated (electron-hole pairs) that are generated in GPFG under light irradiation. These pairs are separated by the internal electric field which only exist at the GOFG-electrode interface [1,2,3]. Then the separated carriers are drifted by an external electric field; hence, an increase in charge carriers 8 resulting in detection action.

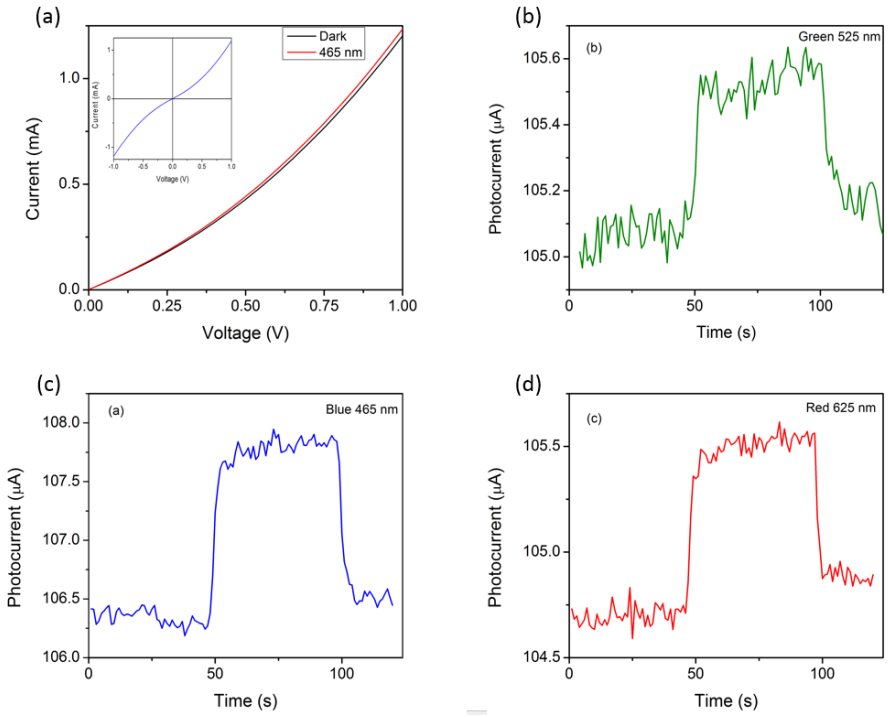

Figure 4-1: I-V and photocurrent characteristic of GOFG/polymer hybrid photodetector. (a) I-V characteristic curve in Dark (black) and under illumination (red) at 465nm wavelength and 100mV bias voltage. The metal-GOFG-metal Schottky-like barrier is shown in the inset. Photocurrent as a function of time at 100 mV under a visible light (a) blue 465 nm, (b) green 525 nm, and (c) red 625 nm.

4.2.2 Reproducibility and selectivity

In order to evaluate the reproducibility of the device, the illumination source was turned on and off repeatedly. Figure 4-2(a) shows the recorded photocurrent with time where photocurrent repeats its behaviour increases directly after the illumination source is turned on, and returns back to its initial value once the light is turned off. The magnitude of photocurrent has no change over all regarding the on/off cycle which indicates that the GOFG photodetector has an excellent behaviour under continuous cycling. In addition, under different light intensities, the photocurrent was measured as a function of time to demonstrate the selectivity of the device under different light intensity. The conductivity of the device decreases with the decrease of the light's irradiation intensity (fig. 4-2 (b)). Fewer photons could be absorbed by GOFG when light intensity is low; hence, fewer electron-hole pairs are generated. Consequently, a smaller photocurrent is produced in the photodetector. Figure 4-2 (c) shows the relation between the photocurrent and the incident light intensity where the relation tends to be exponential as the fitted curve is described by $Y=Y_0+ A*\exp((x-x_0) / t1)$, where Y_0 is the value of dark current and $A*\exp((x-x_0) / t1)$ is the nonlinear term that results from the trapping of carriers by oxygen functional groups [4].

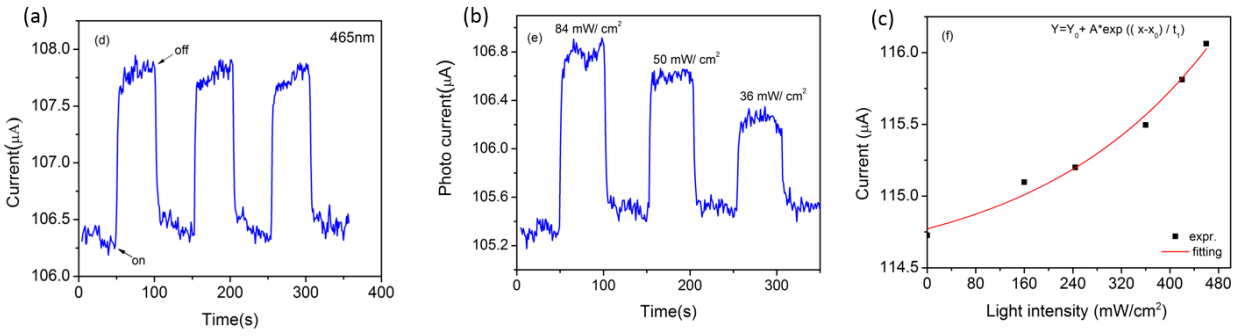

Figure 4-2: Reproducibility and selectivity of GOFG/polymer hybrid photodetector. (a) The photoresponse of GOFG device showing the reproducibility over on-off continuous cycling. (b) The photocurrent of the device as a function of time under different incident-light intensity. (c) Photocurrent as a function of light intensity.

4.2.3 Responsivity and time response

Responsivity (R_λ) and time response which are important figures of merit of the photodetector are calculated. Responsivity (R_λ) is the value of photocurrent that is generated by the intensity of incident light on the effective area of the photodetector [2]. It is defined by the equation [5,6]

$$R_\lambda = I_\lambda / (SP_\lambda)$$

where I_λ is the photocurrent (the difference between illumination current and dark current), S represents the effective area of the device under incident light, P_λ is the intensity of the illumination source, and λ is the light's wavelength. Under a wavelength of 465 nm and 100 mV bais voltage, the responsivity was found to be 0.73 A/W which is considered as a very high responsivity compared to other graphene derivatives-based photodetectors [4,7-12]. Since the GOFG defects ratio is high which influences the scattering of the charge carriers, hence can reduce the conductivity of the device under illumination [4], The high responsivity of the device can be attributed to the design of the device's structure where two important factors, increasing the area of detection and GOFG-electrode end contact, were combined.

Time response is another important factor which can be defined by growth and decay times. Growth time represents the time period from 10% to 90% of the saturated photodetector when the light source is on, while decay time represents the falling time of the photocurrent from 90% to 10% after turning the light off (fig. 4-3) [10]. According to this, the time response was calculated to be 3.4 s and 5.2 s for growth and decay respectively. Once the illumination source is switched off, the excited carriers start recombination. However, the recombination process affected by residual oxygen functional groups and defects [4] in GOFG film result in a larger decay time [12]. Although carrier transport in graphene derivatives is dominated by the disorders and defects in sheets and the coupling between GOFG sheets [13] results in a slow response time compared to intrinsic graphene, GOFG photodetectors exhibit fast time response when compared with many of graphene-derivatives photodetectors. This could be attributed to the GOFG-electrode end contact which results in low contact resistance, resulting in fast carrier transport and a fast response time.

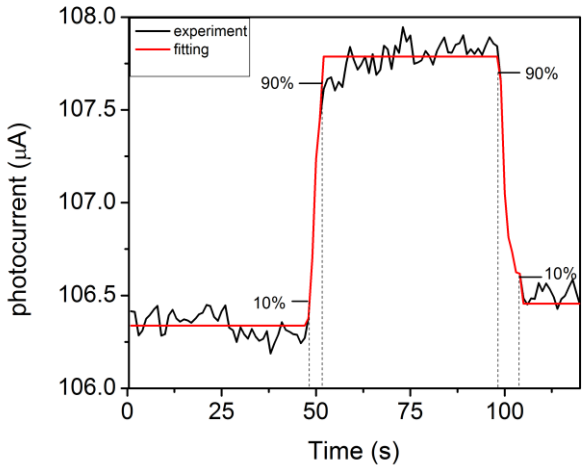

Figure 4-3: The analysis of growth and decay time of the photodetector under visible-blue light 465 nm. The black curve is the experimental data and the red curve is the fitting data.

4.3 Conclusion

Through the experiments carried out for the GOFG/polymer hybrid photodetector performance evaluation, the capability of the device in the detection of visible light was investigated. A remarkable high responsivity and fast response time were observed in the GOFG/polymer hybrid photodetector. Moreover, the device shows a stable reproducibility over continuous cycling of operation, and a significant selectivity for different incident light intensities. This could be attributed to two main factors: i) the design of the device's structure where two important factors, increasing the area of detection and GOFG-electrode end contact, were combined, and ii) the GOFG/polymer hybrid active material that has the ability of stable operation under ambient conditions and reduce the scattering of charge carriers in GOFG sheets.

Chapter 5
Conclusion and future work

5.1 Conclusion

Instability during operation of graphene derivative-based devices is a common drawback in photodetectors that operate in ambient environment. Moreover, the performance of graphene derivative-based devices still are not competitive in the traditional semiconductors photodetectors which increase the importance of engineering the design of device structure or the creation of a new active material. Therefore, in this study, a successful contribution to improve these aspects has been achieved. In the aim of preparing the device to work under ambient conditions, a new hybrid material that consists of graphene oxide femtogel (GOFG) and polymer (poly(methyl methacrylate) PMMA) was prepared and tested as an active material for the first time. In addition, the structure of the device was engineered to contain a large GOFG-metal interface area and GOFG-metal end contact for the first time.

In the GOFG/PMMA hybrid photodetector, a significant operational stability and a remarkably high photoresponsivity was observed. In addition, a fast response time and a high responsivity compared to other graphene derivatives photodetectors have been achieved at low power intensity. Moreover, in comparison between GOFG/PMMA hybrid photodetector and GOFG photodetector, the changing in the sensing mechanism from bolometric to photovoltaic effect has been reported for the first time.

This study could open new avenues in three different aspects that relate to graphene-derivatives sensing devices. First, since putting aqueous solution forms of graphene-derivatives between electrodes in nanoscale is quite a challenge, engineering of this device's structure provides a smooth approach to overcome this problem. Second, it provides a new active material that could be operated in ambient environment with no effect in reliability and stability of the

device. Finally, the method of fabrication and the sensing material of the device can be applied in different sensing applications such as gas sensing and biosensing applications.

5.2 Future work

Since the active material is suitable to be used in other sensing applications, gas sensor use is one of the future plans that can utilize this material. Also, GOFG can be tuned to contain different oxygen functional groups, which means different electrical properties; hence, a variety of targeted applications. Therefore, different forms of GOFG could be used in the future. In addition, more optimization of device structure is another aspect that needs further work.

Bibliography

Chapter 1:

1. Zhan, Z., Zheng, L., Pan, Y., Sun, G., & Li, L. (2012). Self-powered, visible-light photodetector based on thermally reduced graphene oxide–ZnO (rGO–ZnO) hybrid nanostructure. *Journal of Materials Chemistry*, *22*(6), 2589-2595.
2. Bao, Q., & Loh, K. P. (2012). Graphene photonics, plasmonics, and broadband optoelectronic devices. *ACS nano*, *6*(5), 3677-3694.
3. Saleh, B. E. A.; Teich, M. C. Fundamentals of Photonics; John Wiley & Sons: New York, 2007
4. Pickering, J. A. Touch-sensitive screens: the technologies and their applications. Int. J. Man. Mach. Stud. 25, 249–269 (1986).
5. Bonaccorso, F., Sun, Z., Hasan, T., & Ferrari, A. C. (2010). Graphene photonics and optoelectronics. *Nature photonics*, *4*(9), 611-622.
6. Du, X., Skachko, I., Barker, A., & Andrei, E. Y. (2008). Approaching ballistic transport in suspended graphene. *Nature nanotechnology*, *3*(8), 491-495.
7. Morozov, S. V., Novoselov, K. S., Katsnelson, M. I., Schedin, F., Elias, D. C., Jaszczak, J. A., & Geim, A. K. (2008). Giant intrinsic carrier mobilities in graphene and its bilayer. *Physical review letters*, *100*(1), 016602.
8. Nair, R. R., Blake, P., Grigorenko, A. N., Novoselov, K. S., Booth, T. J., Stauber, T., ... & Geim, A. K. (2008). Fine structure constant defines visual transparency of graphene. *Science*, *320*(5881), 1308-1308.
9. Sun, Z., Hasan, T., Torrisi, F., Popa, D., Privitera, G., Wang, F., ... & Ferrari, A. C. (2010). Graphene mode-locked ultrafast laser. *ACS nano*, *4*(2), 803-810.
10. Dawlaty, J. M., Shivaraman, S., Strait, J., George, P., Chandrashekhar, M., Rana, F., ... & Chen, Y. (2008). Measurement of the optical absorption spectra of epitaxial graphene from terahertz to visible. *Applied Physics Letters*, *93*(13), 131905.
11. Wright, A. R., Cao, J. C., & Zhang, C. (2009). Enhanced optical conductivity of bilayer graphene nanoribbons in the terahertz regime. *Physical review letters*, *103*(20), 207401.
12. Novoselov, K. S., Geim, A. K., Morozov, S. V., Jiang, D., Zhang, Y., Dubonos, S. A., ... & Firsov, A. A. (2004). Electric field effect in atomically thin carbon films. *science*, *306*(5696), 666-669.
13. Geim, A. K. (2009). Graphene: status and prospects. *science*, *324*(5934), 1530-1534.
14. Wolf, E. L. (2013). *Graphene: a new paradigm in condensed matter and device physics*. Oxford University Press.

15. Edwards, R. S., & Coleman, K. S. (2013). Graphene synthesis: relationship to applications. *Nanoscale*, *5*(1), 38-51.

16. Wan, X., Huang, Y., & Chen, Y. (2012). Focusing on energy and optoelectronic applications: a journey for graphene and graphene oxide at large scale. *Accounts of chemical research*, *45*(4), 598-607.

17. Schedin, F., Geim, A. K., Morozov, S. V., Hill, E. W., Blake, P., Katsnelson, M. I., & Novoselov, K. S. (2007). Detection of individual gas molecules adsorbed on graphene. *Nature materials*, *6*(9), 652-655.

18. Xia, F., Mueller, T., Lin, Y. M., Valdes-Garcia, A., & Avouris, P. (2009). Ultrafast graphene photodetector. *Nature nanotechnology*, *4*(12), 839-843.

19. Prasai, D., Tuberquia, J. C., Harl, R. R., Jennings, G. K., & Bolotin, K. I. (2012). Graphene: corrosion-inhibiting coating. *ACS nano*, *6*(2), 1102-1108.

20. Guo, C. X., Guai, G. H., & Li, C. M. (2011). Graphene based materials: enhancing solar energy harvesting. *Advanced Energy Materials*, *1*(3), 448-452.

21. Z, E. *Why are Pi bonds weaker than Sigma bonds?* (2014) Available from: http://socratic.org/questions/why-are-pi-bonds-weaker-than-sigma-bonds.

22. Tan, X., Wu, J., Zhang, K., Peng, X., Sun, L., & Zhong, J. (2013). Nanoindentation models and Young's modulus of monolayer graphene: A molecular dynamics study. *Applied Physics Letters*, *102*(7), 071908.

23. Mayorov, A. S., Gorbachev, R. V., Morozov, S. V., Britnell, L., Jalil, R., Ponomarenko, L. A., ... & Geim, A. K. (2011). Micrometer-scale ballistic transport in encapsulated graphene at room temperature. *Nano letters*, *11*(6), 2396-2399.

24. Zhu, W., Zhang, J., & Yu, Z. (2012). Simulation study of channel mobility and device performance dependence on gate stack in graphene field-effect transistors. *Applied Physics Letters*, *100*(11), 112104.

25. Farmer, D. B., Chiu, H. Y., Lin, Y. M., Jenkins, K. A., Xia, F., & Avouris, P. (2009). Utilization of a buffered dielectric to achieve high field-effect carrier mobility in graphene transistors. *Nano letters*, *9*(12), 4474-4478.

26. Peres, N. M. R. (2010). Colloquium: The transport properties of graphene: An introduction. *Reviews of Modern Physics*, *82*(3), 2673.

27. Li, J., Niu, L., Zheng, Z., & Yan, F. (2014). Photosensitive graphene transistors. *Advanced Materials*, *26*(31), 5239-5273.

28. Bao, Q., Zhang, H., Wang, Y., Ni, Z., Yan, Y., Shen, Z. X., ... & Tang, D. Y. (2009). Atomic-layer graphene as a saturable absorber for ultrafast pulsed lasers. *Advanced Functional Materials*, *19*(19), 3077-3083.

29. Mueller, T., Xia, F., & Avouris, P. (2010). Graphene photodetectors for high-speed optical communications. *Nature Photonics*, *4*(5), 297-301.

30. Gabor, N. M., Song, J. C., Ma, Q., Nair, N. L., Taychatanapat, T., Watanabe, K., ... & Jarillo-Herrero, P. (2011). Hot carrier–assisted intrinsic photoresponse in graphene. *Science*, *334*(6056), 648-652.

31. Song, J. C., Rudner, M. S., Marcus, C. M., & Levitov, L. S. (2011). Hot carrier transport and photocurrent response in graphene. *Nano letters*, *11*(11), 4688-4692.

32. Yan, J., Kim, M. H., Elle, J. A., Sushkov, A. B., Jenkins, G. S., Milchberg, H. W. M., ... & Drew, H. D. (2012). Dual-gated bilayer graphene hot-electron bolometer. *Nature nanotechnology*, *7*(7), 472-478.

33. Freitag, M., Low, T., Xia, F., & Avouris, P. (2013). Photoconductivity of biased graphene. *Nature Photonics*, *7*(1), 53-59.

34. Koppens, F. H. L., Mueller, T., Avouris, P., Ferrari, A. C., Vitiello, M. S., & Polini, M. (2014). Photodetectors based on graphene, other two-dimensional materials and hybrid systems. *Nature nanotechnology*, *9*(10), 780-793.

35. Schniepp, H. C., Li, J. L., McAllister, M. J., Sai, H., Herrera-Alonso, M., Adamson, D. H., ... & Aksay, I. A. (2006). Functionalized single graphene sheets derived from splitting graphite oxide. *The Journal of Physical Chemistry B*, *110*(17), 8535-8539.

36. Hummers Jr, W. S., & Offeman, R. E. (1958). Preparation of graphitic oxide.*Journal of the American Chemical Society*, *80*(6), 1339-1339.

37. Kurra, N., Bhadram, V. S., Narayana, C., & Kulkarni, G. U. (2013). Few layer graphene to graphitic films: infrared photoconductive versus bolometric response. *Nanoscale*, *5*(1), 381-389.

38. Chang, H., Sun, Z., Saito, M., Yuan, Q., Zhang, H., Li, J., ... & Yan, F. (2013). Regulating infrared photoresponses in reduced graphene oxide phototransistors by defect and atomic structure control. *ACS nano*, *7*(7), 6310-6320.

39. Chang, H., Sun, Z., Yuan, Q., Ding, F., Tao, X., Yan, F., & Zheng, Z. (2010). Thin Film Field-Effect Phototransistors from Bandgap-Tunable, Solution-Processed, Few-Layer Reduced Graphene Oxide Films. *Advanced Materials*,*22*(43), 4872-4876.

40. Chitara, B., Panchakarla, L. S., Krupanidhi, S. B., & Rao, C. N. R. (2011). Infrared photodetectors based on reduced graphene oxide and graphene nanoribbons. *Advanced Materials*, *23*(45), 5419-5424.

41. Lai, S. K., Tang, L., Hui, Y. Y., Luk, C. M., & Lau, S. P. (2014). A deep ultraviolet to near-infrared photoresponse from glucose-derived graphene oxide. *Journal of Materials Chemistry C*, *2*(34), 6971-6977.

42. Lian, K. Y., Ji, Y. F., Li, X. F., Jin, M. X., Ding, D. J., & Luo, Y. (2013). Big bandgap in highly reduced graphene oxides. *The Journal of Physical Chemistry C*, *117*(12), 6049-6054.

43. Mathkar, A., Tozier, D., Cox, P., Ong, P., Galande, C., Balakrishnan, K., ... & Ajayan, P. M. (2012). Controlled, stepwise reduction and band gap manipulation of graphene oxide. *The journal of physical chemistry letters*,*3*(8), 986-991.

44. Kobayashi, T., Kimura, N., Chi, J., Hirata, S., & Hobara, D. (2010). Channel-Length-Dependent Field-Effect Mobility and Carrier Concentration of Reduced Graphene Oxide Thin-Film Transistors. *Small*, *6*(11), 1210-1215.

45. Zhu, Y., Murali, S., Cai, W., Li, X., Suk, J. W., Potts, J. R., & Ruoff, R. S. (2010). Graphene and graphene oxide: synthesis, properties, and applications. *Advanced materials*, *22*(35), 3906-3924.

46. Park, S., & Ruoff, R. S. (2009). Chemical methods for the production of graphenes. *Nature nanotechnology*, *4*(4), 217-224.

Chapter 2:

1. Chang, H., Sun, Z., Yuan, Q., Ding, F., Tao, X., Yan, F., & Zheng, Z. (2010). Thin Film Field-Effect Phototransistors from Bandgap-Tunable, Solution-Processed, Few-Layer Reduced Graphene Oxide Films. *Advanced Materials*,*22*(43), 4872-4876
2. Chitara, B., Panchakarla, L. S., Krupanidhi, S. B., & Rao, C. N. R. (2011). Infrared photodetectors based on reduced graphene oxide and graphene nanoribbons. *Advanced Materials*, *23*(45), 5419-5424
3. Chang, H., Sun, Z., Saito, M., Yuan, Q., Zhang, H., Li, J., ... & Yan, F. (2013). Regulating infrared photoresponses in reduced graphene oxide phototransistors by defect and atomic structure control. *ACS nano*, *7*(7), 6310-6320.
4. Xia, F., Mueller, T., Lin, Y. M., Valdes-Garcia, A., & Avouris, P. (2009). Ultrafast graphene photodetector. *Nature nanotechnology*, *4*(12), 839-843.
5. Park, S., & Ruoff, R. S. (2009). Chemical methods for the production of graphenes. *Nature nanotechnology*, *4*(4), 217-224.
6. Li, D., Mueller, M. B., Gilje, S., Kaner, R. B., & Wallace, G. G. (2008). Processable aqueous dispersions of graphene nanosheets. *Nature nanotechnology*, *3*(2), 101-105.
7. Chitara, B., Krupanidhi, S. B., & Rao, C. N. R. (2011). Solution processed reduced graphene oxide ultraviolet detector. *Applied Physics Letters*, *99*(11), 113114.
8. Chowdhury, F. A., Mochida, T., Otsuki, J., & Alam, M. S. (2014). Thermally reduced solution-processed graphene oxide thin film: An efficient infrared photodetector. *Chemical Physics Letters*, *593*, 198-203.
9. Ghosh, S., Sarker, B. K., Chunder, A., Zhai, L., & Khondaker, S. I. (2010). Position dependent photodetector from large area reduced graphene oxide thin films. *Applied Physics Letters*, *96*(16), 163109.

10. Lai, S. K., Tang, L., Hui, Y. Y., Luk, C. M., & Lau, S. P. (2014). A deep ultraviolet to near-infrared photoresponse from glucose-derived graphene oxide. *Journal of Materials Chemistry C*, *2*(34), 6971-6977.
11. Qi, X., Zou, X., Huang, Z., Ren, L., Hao, G., Liu, Y., ... & Zhong, J. (2013). Ultraviolet, visible, and near infrared photoresponse properties of solution processed graphene oxide. *Applied Surface Science*, *266*, 332-336.
12. Mueller, T., Xia, F., & Avouris, P. (2010). Graphene photodetectors for high-speed optical communications. *Nature Photonics*, *4*(5), 297-301.
13. Bonaccorso, F., Sun, Z., Hasan, T., & Ferrari, A. C. (2010). Graphene photonics and optoelectronics. *Nature photonics*, *4*(9), 611-622.
14. Xia, F., Mueller, T., Lin, Y. M., Valdes-Garcia, A., & Avouris, P. (2009). Ultrafast graphene photodetector. *Nature nanotechnology*, *4*(12), 839-843.
15. Ibrahim, K. M. (2015). Femtosecond Laser Interaction with Graphene Oxide Aqueous Solution. University of Waterloo, Waterloo, Ontario, Canada
16. Bai, J., Duan, X., & Huang, Y. (2009). Rational fabrication of graphene nanoribbons using a nanowire etch mask. *Nano letters*, *9*(5), 2083-2087.
17. Prado, M. C., Jariwala, D., Marks, T. J., & Hersam, M. C. (2013). Optimization of graphene dry etching conditions via combined microscopic and spectroscopic analysis. *Applied Physics Letters*, *102*(19), 193111.
18. Chen, Z., Lin, Y. M., Rooks, M. J., & Avouris, P. (2007). Graphene nano-ribbon electronics. *Physica E: Low-dimensional Systems and Nanostructures*, *40*(2), 228-232.
19. Wang, X., & Dai, H. (2010). Etching and narrowing of graphene from the edges. *Nature chemistry*, *2*(8), 661-665.
20. Xie, L., Jiao, L., & Dai, H. (2010). Selective etching of graphene edges by hydrogen plasma. *Journal of the American Chemical Society*, *132*(42), 14751-14753.
21. Kudin, K. N., Ozbas, B., Schniepp, H. C., Prud'Homme, R. K., Aksay, I. A., & Car, R. (2008). Raman spectra of graphite oxide and functionalized graphene sheets. *Nano letters*, *8*(1), 36-41.
22. Moon, I. K., Lee, J., Ruoff, R. S., & Lee, H. (2010). Reduced graphene oxide by chemical graphitization. *Nature communications*, *1*, 73.

Chapter 3:

1. Trung, T. Q., Tien, N. T., Kim, D., Jung, J. H., Yoon, O. J., & Lee, N. E. (2012). High Thermal Responsiveness of a Reduced Graphene Oxide Field-Effect Transistor. *Advanced Materials*, *24*(38), 5254-5260.

2. Jung, I., Dikin, D., Park, S., Cai, W., Mielke, S. L., & Ruoff, R. S. (2008). Effect of water vapor on electrical properties of individual reduced graphene oxide sheets. *The Journal of Physical Chemistry C*, *112*(51), 20264-20268.

3. Kim, W., Javey, A., Vermesh, O., Wang, Q., Li, Y., & Dai, H. (2003). Hysteresis caused by water molecules in carbon nanotube field-effect transistors. *Nano Letters*, *3*(2), 193-198.

4. Lohmann, Timm, Klaus von Klitzing, and Jurgen H. Smet. "Four-terminal magneto-transport in graphene pn junctions created by spatially selective doping." *Nano letters* 9.5 (2009): 1973-1979.

5. Kobayashi, T., Kimura, N., Chi, J., Hirata, S., & Hobara, D. (2010). Channel-Length-Dependent Field-Effect Mobility and Carrier Concentration of Reduced Graphene Oxide Thin-Film Transistors. *Small*, *6*(11), 1210-1215.

6. Yun, J. M., Park, S., Hwang, Y. H., Lee, E. S., Maiti, U., Moon, H., ... & Kim, S. O. (2013). Complementary p-and n-Type Polymer Doping for Ambient Stable Graphene Inverter. *ACS nano*, *8*(1), 650-656.

7. Zhu, W., Zhang, J., & Yu, Z. (2012). Simulation study of channel mobility and device performance dependence on gate stack in graphene field-effect transistors. *Applied Physics Letters*, *100*(11), 112104.

8. Farmer, D. B., Chiu, H. Y., Lin, Y. M., Jenkins, K. A., Xia, F., & Avouris, P. (2009). Utilization of a buffered dielectric to achieve high field-effect carrier mobility in graphene transistors. *Nano letters*, *9*(12), 4474-4478.

9. Chen, J. H., Jang, C., Xiao, S., Ishigami, M., & Fuhrer, M. S. (2008). Intrinsic and extrinsic performance limits of graphene devices on SiO2.*Nature nanotechnology*, *3*(4), 206-209.

10. Chang, H., Sun, Z., Yuan, Q., Ding, F., Tao, X., Yan, F., & Zheng, Z. (2010). Thin Film Field-Effect Phototransistors from Bandgap-Tunable, Solution-Processed, Few-Layer Reduced Graphene Oxide Films. *Advanced Materials*,*22*(43), 4872-4876.

11. Chitara, B., Krupanidhi, S. B., & Rao, C. N. R. (2011). Solution processed reduced graphene oxide ultraviolet detector. *Applied Physics Letters*, *99*(11), 113114.

12. Pham, V. H., Dang, T. T., Hur, S. H., Kim, E. J., & Chung, J. S. (2012). Highly conductive poly (methyl methacrylate)(PMMA)-reduced graphene oxide composite prepared by self-assembly of PMMA latex and graphene oxide through electrostatic interaction. *ACS applied materials & interfaces*,*4*(5), 2630-2636.

13. Chitara, B., Panchakarla, L. S., Krupanidhi, S. B., & Rao, C. N. R. (2011). Infrared photodetectors based on reduced graphene oxide and graphene nanoribbons. *Advanced Materials*, *23*(45), 5419-5424

14. Chang, H., Sun, Z., Saito, M., Yuan, Q., Zhang, H., Li, J., ... & Yan, F. (2013). Regulating infrared photoresponses in reduced graphene oxide phototransistors by defect and atomic structure control. *ACS nano*, *7*(7), 6310-6320

15. Lai, S. K., Tang, L., Hui, Y. Y., Luk, C. M., & Lau, S. P. (2014). A deep ultraviolet to near-infrared photoresponse from glucose-derived graphene oxide. *Journal of Materials Chemistry C*, *2*(34), 6971-6977.

16. Kurra, N., Bhadram, V. S., Narayana, C., & Kulkarni, G. U. (2013). Few layer graphene to graphitic films: infrared photoconductive versus bolometric response. *Nanoscale*, *5*(1), 381-389.

17. Chitara, B., Krupanidhi, S. B., & Rao, C. N. R. (2011). Solution processed reduced graphene oxide ultraviolet detector. *Applied Physics Letters*, *99*(11), 113114.

18. Yan, J., Kim, M. H., Elle, J. A., Sushkov, A. B., Jenkins, G. S., Milchberg, H. W. M., ... & Drew, H. D. (2012). Dual-gated bilayer graphene hot-electron bolometer. *Nature nanotechnology*, *7*(7), 472-478.

19. Freitag, M., Low, T., Xia, F., & Avouris, P. (2013). Photoconductivity of biased graphene. *Nature Photonics*, *7*(1), 53-59.

20. Xia, F., Mueller, T., Lin, Y. M., Valdes-Garcia, A., & Avouris, P. (2009). Ultrafast graphene photodetector. *Nature nanotechnology*, *4*(12), 839-843.

21. Liu, C. H., Chang, Y. C., Norris, T. B., & Zhong, Z. (2014). Graphene photodetectors with ultra-broadband and high responsivity at room temperature. *Nature nanotechnology*, *9*(4), 273-278.

22. Rao, G., Freitag, M., Chiu, H. Y., Sundaram, R. S., & Avouris, P. (2011). Raman and photocurrent imaging of electrical stress-induced p–n junctions in graphene. *ACS nano*, *5*(7), 5848-5854.

23. Mueller, T., Xia, F., Freitag, M., Tsang, J., & Avouris, P. (2009). Role of contacts in graphene transistors: A scanning photocurrent study. *Physical Review B*, *79*(24), 245430.

24. Koppens, F. H. L., Mueller, T., Avouris, P., Ferrari, A. C., Vitiello, M. S., & Polini, M. (2014). Photodetectors based on graphene, other two-dimensional materials and hybrid systems. *Nature nanotechnology*, *9*(10), 780-793.

Chapter 4:

1. Mueller, T., Xia, F., & Avouris, P. (2010). Graphene photodetectors for high-speed optical communications. *Nature Photonics*, *4*(5), 297-301.

2. Bonaccorso, F., Sun, Z., Hasan, T., & Ferrari, A. C. (2010). Graphene photonics and optoelectronics. *Nature photonics*, *4*(9), 611-622.

3. Xia, F., Mueller, T., Lin, Y. M., Valdes-Garcia, A., & Avouris, P. (2009). Ultrafast graphene photodetector. *Nature nanotechnology*, *4*(12), 839-843.
4. Chang, H., Sun, Z., Saito, M., Yuan, Q., Zhang, H., Li, J., ... & Yan, F. (2013). Regulating infrared photoresponses in reduced graphene oxide phototransistors by defect and atomic structure control. *ACS nano*, *7*(7), 6310-6320.
5. Ueda, T., An, Z., Hirakawa, K., & Komiyama, S. (2008). Charge-sensitive infrared phototransistors: Characterization by an all-cryogenic spectrometer.*Journal of Applied Physics*, *103*(9), 3109.
6. Cheng, J., Zhang, Y., & Guo, R. (2008). ZnO microtube ultraviolet detectors.*Journal of Crystal Growth*, *310*(1), 57-61.
7. Chitara, B., Krupanidhi, S. B., & Rao, C. N. R. (2011). Solution processed reduced graphene oxide ultraviolet detector. *Applied Physics Letters*, *99*(11), 113114.
8. Chitara, B., Panchakarla, L. S., Krupanidhi, S. B., & Rao, C. N. R. (2011). Infrared photodetectors based on reduced graphene oxide and graphene nanoribbons. *Advanced Materials*, *23*(45), 5419-5424.
9. Chowdhury, F. A., Mochida, T., Otsuki, J., & Alam, M. S. (2014). Thermally reduced solution-processed graphene oxide thin film: An efficient infrared photodetector. *Chemical Physics Letters*, *593*, 198-203.
10. Lai, S. K., Tang, L., Hui, Y. Y., Luk, C. M., & Lau, S. P. (2014). A deep ultraviolet to near-infrared photoresponse from glucose-derived graphene oxide. *Journal of Materials Chemistry C*, *2*(34), 6971-6977.
11. Ghosh, S., Sarker, B. K., Chunder, A., Zhai, L., & Khondaker, S. I. (2010). Position dependent photodetector from large area reduced graphene oxide thin films. *Applied Physics Letters*, *96*(16), 163109.
12. Qi, X., Zou, X., Huang, Z., Ren, L., Hao, G., Liu, Y., ... & Zhong, J. (2013). Ultraviolet, visible, and near infrared photoresponse properties of solution processed graphene oxide. *Applied Surface Science*, *266*, 332-336.
13. Trung, T. Q., Tien, N. T., Kim, D., Jung, J. H., Yoon, O. J., & Lee, N. E. (2012). High Thermal Responsiveness of a Reduced Graphene Oxide Field-Effect Transistor. *Advanced Materials*, *24*(38), 5254-5260.